Exploration of the Defect's Effect on the Mechanical Properties of Different Orientated Nanowires

H.F. Zhan[a] and Y.T. Gu[b]

School of Engineering Systems, Queensland University of Technology,

Brisbane, QLD 4001, Australia

[a]zhan.haifei@qut.edu.au, [b]yuantong.gu@qut.edu.au

Keywords: Nanowires, Defect, Orientation, Deformation Mechanism, Molecular Dynamics

Abstract. Molecular dynamics (MD) simulations have been carried out to investigate the defect's effect on the mechanical properties of copper nanowire with different crystallographic orientations, under tensile deformation. Three different crystallographic orientations have been considered. The deformation mechanism has been carefully discussed. It is found that the Young's modulus is insensitive to the defect, even when the nanowire's crystallographic orientation is different. However, due to the defect's effect, the yield strength and yield strain appear a large decrease. The defects have played a role of dislocation sources, the slips or stacking faults are first generated around the locations of the defects. The necking locations have also been affected by different defects. Due to the surface defect, the plastic deformation has received a large influence for the $<001>/\{110\}$ and $<110>$ orientated nanowires, and a relative small influence is seen for the $<111>$ nanowire.

Introduction

Nanowires have become the focus of intensive research, owing to their distinct mechanical, electrical, optical and other properties that arise from their nanometre size scale and possible quantum confinement [1]. They have gained immense applications as the active components of nanoelectromechanical systems (NEMS) including high frequency resonator, force and pressure sensing, and others devices [2]. Massive numerical studies have been dedicated to explore the revolutionary characteristics of nanowires. For example, great deals of numerical studies have been carried out to investigate mechanical properties of nanowires under uniaxial loading condition. Ikeda et al [3] demonstrated that a homogeneous perfect crystal at constant temperature can be transformed to an amorphous metal under large strain rates. The buckling behaviour of single-crystal silicon nanowire under compression has been studied by Jing et al [4]. Other mechanical behaviours study such as bending deformation [5], torsion deformation [6] have been reported.

Due to the significant surface-to-volume ratio, the surfaces exert great effects on the structure and properties of nanowires [7]. For example, gold nanowire with the $<100>$ initial crystallographic orientation and wire cross-sectional area below 4 nm^2, is found transformed from FCC structure to body-centred-tetragonal (BCT) structure [8]. Single and multi-step phase transformation in CuZr nanowire under compressive/tensile loading is reported by Sutrakar et al [9]. Recently, some researchers reported the shape memory and pseudoelasticity phenomenon in Au, Cu, Ni, and Ag and NiAl nanowires [10], which reveals the crystallographic orientation can exert enormous influence to nanowire's properties. Nanowires that grown in different crystallographic orientations have been reported by several researchers [11, 12]. Accordingly, some recent works have been carried out to explore the mechanical behaviours of nanowires with different crystallographic orientations under uniaxial loading condition [13]. For instance, Park et al [14] studied the propensity of the FCC nanowires to deform via twinning or slip under compressive/tensile loading.

Because of the nanometre size scale, the presence of defects is one of the most influential factors in determining the nanomaterials' properties. For example, significant stress concentrations can occur at the tip of notches in the surfaces, which would eventually result the propagation of cracks through the system and degradation of mechanical behaviour [15]. Thus, studying the defect's effect is crucial to enhance the utility of nanoscale materials. Unfortunately, the experimental study of the defect's effect on nanowires suffers significant difficulty and the numerical simulation plays a critical role for it. Several numerical studies of the defects on nanowires have been reported, such as the study of the grain boundaries effect on the mechanical tensile behaviour of twinned metal nanowires [16]. However, to the best of authors knowledge, there is still no numerical study of the defect's effect on the nanowire's properties with different crystallographic orientations.

Therefore, in this work, we will apply the molecular dynamics (MD) simulation to explore the deformation mechanism of defected copper nanowires with different orientations under tensile deformation. Since mechanical properties of the nanowire are greatly influenced by the surface effect, the defects located on the surface will be considered. Three groups of simulations with different crystallographic orientations will be carried out and the deformation mechanisms in each group will be discussed.

Numerical Implementation

MD simulations are carried out on single-crystal copper nanowires under the tensile deformation. The simulation models with different crystallographic orientations are chosen according to previous researchers [14, 17]. Three groups with two cases (a perfect case and a defect case) in each group have been considered. The same size is applied in each group with all three groups have the approximate same size. Simulation models are shown in Fig. 1, including: Case a and b in Group 1 with the size of $2.553\times2.553\times10.83nm^3$; Case c and d in Group 2 with the size of $2.35\times2.552\times11.255nm^3$; Case e and f in Group 3 with the size of $2.358\times2.501\times11.232nm^3$.

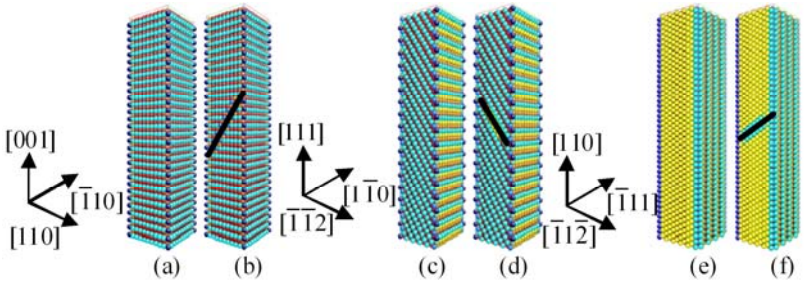

Fig. 1. Different simulation models: Group 1: (a) Perfect <001>/{110} nanowire; (b) Defected <001>/{110} nanowire; Group 2: (c) Perfect <111> nanowire; (d) Defected <111> nanowire; Group 3: (e) Perfect <110> nanowire; (f) Defected <110> nanowire. The surface defects are highlighted by the tilt lines in figures (b), (d) and (f).

The surface defects in Case b, d and f are generated by removing the same amount of atoms in side surface. Periodic boundary condition is applied in the longitudinal direction with other two directions of free surfaces. The nanowire is first relaxed to a minimum energy state using conjugate gradient energy minimization and then the Nose-Hoover thermostat [18, 19] is employed to equilibrate the nanowires at 0.01K. As reported by previous researchers, at high strain rate $(>10^{10}s^{-1})$, the metal nanowire will transform to an amorphous state and undergo homogeneous deformation flow. To avoid such a deformation process, a relative slow constant strain rate of $5\times10^{8}s^{-1}$ will be applied.

The embedded-atom-method (EAM) potential developed for copper by Mishin [20] is used to describe the atomic interactions during these simulations and the equations of motion are integrated with time using a Velocity Verlet algorithm [21]. In order to analyse the partial dislocation and

stacking faults (SFs) during the tensile deformation, the centro-symmetry parameter (*csp*) is used [22], which increases from 0 for perfect FCC lattice to positive values for defects and for atoms close to free surfaces. During this work, $0.5 < csp \le 3, 3 < csp \le 12$, and $csp > 12$ will be assigned to identify the partial dislocations, SFs and surface atoms, respectively.

Deformation Mechanisms Analysis

Fig. 2 shows the stress-strain curves of the six cases subject to uniaxial tensile loading. It is apparent that, all six nanowires deform elastically until reaching the yield point. Case *c* appears the largest yield strength as 12.92 GPa, with Case *d* only about 5.902 GPa and the different slops of the stress-strain curves reveal that the perfect $<111>$ nanowire has the largest Young's modulus, which suggests the obvious influence of the crystallographic orientation on the nanowire's properties. In each group, the elastic region of the stress-strain curves are found coincident, means the Young's modulus is insensitive to the surface defect. However, due to the existence of surface defect, an obvious decrease of the yield strength is found for these three groups. Particularly, in Group 1, the yield strength of Case *a* is around 9.125 GPa, with a smaller value around 7.996 GPa for Case *b*, indicating a 12.37% decrease. Generally, the above results are consistent with our previous findings of the $<001>/\{100\}$ nanowire [23]. To investigate in detail about the combination effect of the surface defect and the crystallographic orientation, a deep discussion of the deformation mechanisms of these three groups is present in the following part. Atomic configurations at different strain points are chosen to best clarify the deformation process of the nanowire.

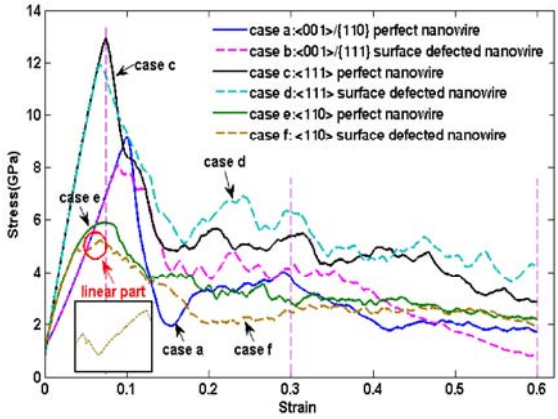

Fig. 2. Stress-strain curves of the different orientated nanowires.

$<001>/\{110\}$ Nanowire. Fig. 3 shows the atomic configurations of Group 1 at three different strain points. According to the first and second columns of Fig. 3, Case *a* appears a very interesting deformation process. After yielding, atoms located on one edge of the nanowire have involved in a rearrangement, with no specific slips as illustrated in Fig. 3(a1). With further deformation, the rearrangement process propagated to the entire cross-section, leaving a completely changed structure. The original (001) longitudinal surfaces are found transformed to {111} surfaces in Fig. 3B, and only two different layers are found in Fig. 3A repeated along the longitudinal direction, which suggests that, the nanowire has changed into a HCP structure. In particular, after this deformation process, at the strain of 0.184, a shield-like cross-section is formed, as shown in Fig. 3B. Actually, the orientations of the HCP structure of the nanowire are changing with further elongation. As the entire nanowire has involved in such a reorientation process, which is totally different from a traditional slip dominated plastic deformation, therefore, we refer this period of deformation as a phase transformation process. At the strain around 0.284, the nanowire begins to resume to the FCC structure, with the side surfaces as the {111} planes, and the longitudinal surfaces as {110} planes. Similar as demonstrated by Liang and Zhou [24], the $<110>/\{111\}$

orientation is energetically favoured for the nanowire's reorientation. When the strain reaches 0.6, only a small fraction of SFs layers are still exist, as seen in Fig. 3(a3). It is interested to mention that the cross-section of the nanowire is still shield-like, as shown in Fig. 3C. This is reasonable, as the side surfaces of the nanowire are all {111} planes, which have eventually constituted a shield-like cross-section and the value of the angles equal the angles between two different {111} planes. In addition, at the strain of 0.6, the necking phenomenon has also been observed.

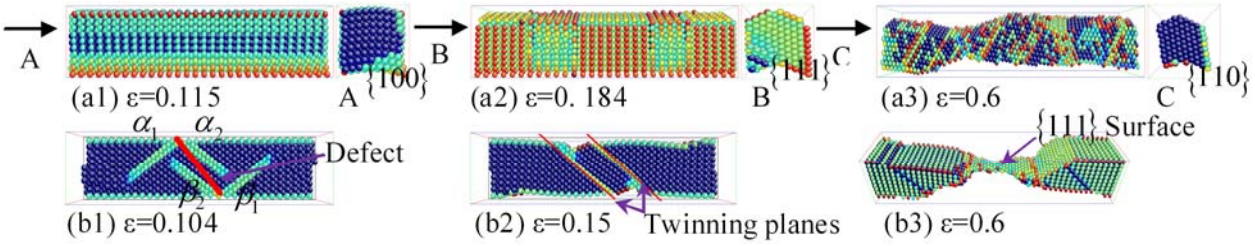

Fig. 3. Atomic configurations of Group 1: (a1)~(a3) are perfect nanowire; (b1)~(b3) are defected nanowire. All the figures are visualized according to the *csp* value between 0~12. Left views of (a1)~(a3) are provided as A, B and C; (b1) and (b2) are sectional views.

Although Case b shares the same orientation as Case a, we find the deformation process appears totally different. According to Fig. 3(b1), instead of the phase transformation in the perfect nanowire, two V-like intrinsic SFs ($\alpha_1,\alpha_2,\beta_1,\beta_2$) are observed generating around two ends of the defect after yielding. After further elongation, α_1 and β_1 are found disappeared, and a twin is generated due to the interaction of α_2 and β_2. Two parallel SFs layers are found, as illustrated in Fig. 3(b2), which are the twinning planes. According to Fig. 3(b3), we find the middle part of the nanowire undertakes most of the deformation, which is also the location of necking. Especially, no SFs layer is observed and the surface around the necking is a {111} plane. Comparing with the structure of the perfect nanowire at the strain of 0.6, we find the whole structure of the defected nanowire is still well organized. In summary, a great influence on the deformation mechanism of the $<001>/\{110\}$ nanowire is observed due to the existence of surface defect during tensile deformation.

$<111>$ Nanowire. Fig. 4 shows the atomic configurations of Group 2 at three different strain points. Basically, the deformation processes of these two cases exhibit very similar with each other. For Case c, several parallel intrinsic SFs are first generated after yielding as shown in Fig. 4(c1). As the longitudinal surface of the nanowire is {111} planes, therefore, according to the Thompson's tetrahedron, other three {111} planes share the same angles with the length direction, indicating they should be equally favoured for the slip. This assumption is approved with further deformation, and the intrinsic SFs are found in other two {111} planes, as illustrated in Fig. 4(c2). When the strain reaches 0.6, only a few of intrinsic SFs are left, which suggests that the perfect $\{111\}<110>$ slip is accomplished by two sequential $\{111\}<112>$ partial slips that occur on the same {111} plane. From Fig. 4(c3), the necking is found located at the middle of the nanowire. For Case d, two parallel intrinsic SFs are first emerged from two ends of the defect, and propagated to the surface, as illustrated in Fig. 4(d1). Similar as the perfect case, intrinsic SFs are generated in other {111} slip planes after further deformation. From Fig. 4(d3), we find that, there is still no obvious necking at the strain of 0.6. This is also implied by the stress-strain curve in Fig. 2, which shows Case d has the largest stress at the strain of 0.6. In all, the surface defect exerts less effect to the deformation mechanism in this group, and the slip dominated deformation process is observed in these two cases.

$<110>$ Nanowire. Fig. 5 shows the atomic configurations of Group 3 at three different strain points. Generally, Case e and f reveal different deformation processes. For Case e, a number of parallel SFs are generated after yielding, with only one intrinsic SFs λ_1 is found in a different $\{111\}$

plane at the left end of the nanowire, which intersects with λ_2, as highlighted by the rectangle in Fig. 5(e1). Especially, these parallel SFs are mainly intrinsic SFs, and they divide the nanowire into several equal sections. With further elongation, we find the movement of the left layer of SFs λ_2, which, in the one hand, cased the annihilation of the oppose SFs λ_1, and in the other hand, induced a twin behind its track, as illustrated in Fig. 5(e2). From Fig. 5(e3), we find that only a small fraction of twins are remained at the strain of 0.6, and the necking location is supposed to be the right end of the nanowire.

Different from Case *e*, only one intrinsic SFs is found generated around the surface defect in Case *f*, as shown in Fig. 5(f1). Afte the formation of this SFs, a relative stable deforamtion process is observed, with no obvious dislocations generation or movements activities. This process has contributed to an approximate linear part in the stress-strain curve, as pointed out in Fig. 2. With further elogation, the two layers of the intrinsic SFs propagate in opposite directions, which produces a twin between them, as shown in Fig. 5(f2). In particular, this twinning process almost goes through the entire nanowire, which changes the original $(\bar{1}11)$ side surfaces to {100} surfaces. According to Fig. 5(f3), we find only a small part of the nanowire is still in the origianl orientation at the strain of 0.6. The necking position is observed at the middle of the nanowire. In short, we find the slips and twins deforamtion process in this group and a large influence is resulted from the surface defect.

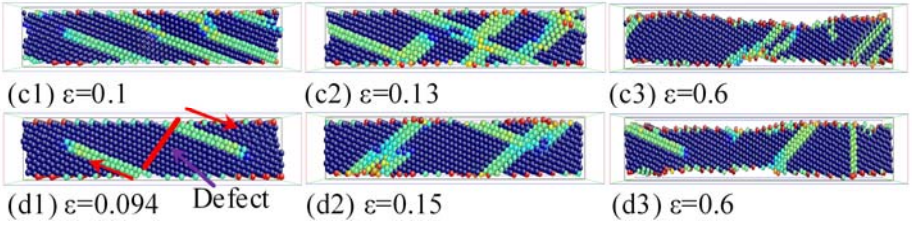

Fig. 4. Atomic configurations of Group 2: (c1)~(c3) are perfect nanowire; (d1)~(d3) are defected nanowire. Atoms with the *csp* value between 0~12 are visualized; all figures are sectional views.

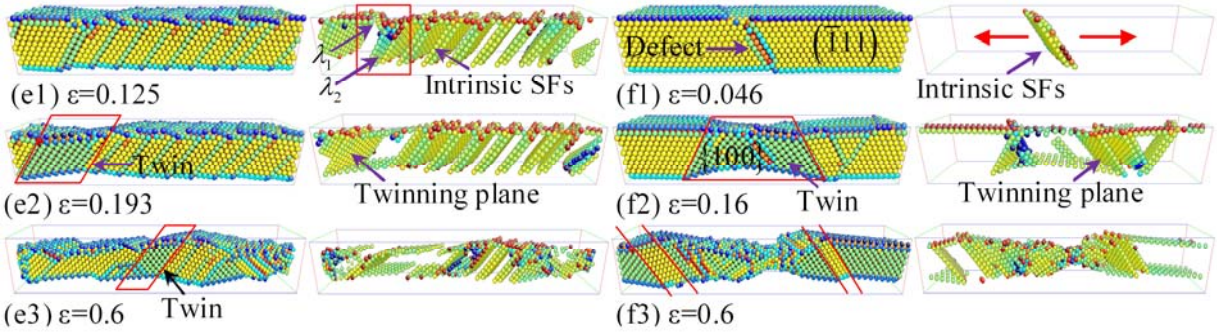

Fig. 5. Atomic configurations of Group 3: (e1)~(e3) are perfect nanowire; (f1)~(f3) are defected nanowire. The left and right figures of each group are visualized according to the *csp* value between 0.5~10 and the coordination number between 4~12, respectively.

Conclusions

MD simulations have been carried out to investigate the defect's effect on the mechanical properties of copper nanowire with different crystallographic orientations, under tensile deformation. Three different crystallographic orientations have been considered. The deformation mechanism has been carefully examined, and the main conclusions are drawn as follows:

(1). Nanowires with different crystallographic orientations appear different mechanical behaviours under tensile deformation, and a larger Young's modulus is found for the $<111>$ nanowire, comparing the nanowires with other two orientations.
(2). The Young's modulus is found insensitive to the defect, even when the nanowire's crystallographic orientation is different. However, a large decrease is observed for the yield strength.
(3). The defects are found as a role of dislocation sources, the slips or SFs layers are first generated around the locations of the defects. The necking locations have also been affected due to different defects.
(4). The surface defects exert large influence on the plastic deformation of the $<001>/\{110\}$ and $<110>$ orientated nanowires, and a relative small influence is seen for the $<111>$ nanowire. In particular, for the perfect $<110>$ nanowire, a combined slip and twinning deformation process is observed. In the opposite, only twinning deformation process is found for the surface defected $<110>$ nanowire.

Conclusively, this study provides a fundamental understanding of different orientated nanowires tensile behaviours when there are surface defects presented, which will enrich the current study of nanowires.

References

[1] J. Sarkar, G. Khan, A. Basumallick, Bull. Mater. Sci., 30 (2007) 271-290.
[2] D. Rugar, R. Budakian, H. Mamin, B. Chui, Nature, 430 (2004) 329-332.
[3] H. Ikeda, Y. Qi, T. Çagin, K. Samwer, W.L. Johnson, W.A. Goddard, Phys. Rev. Lett., 82 (1999) 2900.
[4] Y. Jing, Q. Meng, Y. Gao, Comput. Mater. Sci., 45 (2009) 321-326.
[5] M. McDowell, A. Leach, K. Gall, Modell. Simul. Mater. Sci. Eng., 16 (2008) 045003.
[6] S. Jiang, H. Zhang, Y. Zheng, Z. Chen, J. Phys. D: Appl. Phys., 42 (2009) 135408.
[7] M. McDowell, A. Leach, K. Gall, Nano Lett., 8 (2008) 3613-3618.
[8] K. Gall, J. Diao, M.L. Dunn, M. Haftel, N. Bernstein, M.J. Mehl, J. Eng. Mater. Technol., 127 (2005) 417.
[9] V.K. Sutrakar, D.R. Mahapatra, Intermetallics, 18 (2010) 679-687.
[10] H.S. Park, Nano Lett., 6 (2006) 958-962.
[11] J. Liu, J. Duan, M. Toimil-Molares, S. Karim, T. Cornelius, D. Dobrev, H. Yao, Y. Sun, M. Hou, D. Mo, Nanotechnology, 17 (2006) 1922.
[12] R. Dou, B. Derby, Scripta Mater., 59 (2008) 151-154.
[13] Y. Lin, D. Pen, Nanotechnology, 18 (2007) 395705.
[14] H. Park, K. Gall, J. Zimmerman, J. Mech. Phys. Solids, 54 (2006) 1862-1881.
[15] S. Tyagi, J. Lee, G. Buxton, A. Balazs, Macromolecules, 37 (2004) 9160-9168.
[16] A. Cao, Y. Wei, E. Ma, Phys. Rev. B, 77 (2008) 195429.
[17] J. Diao, K. Gall, M. Dunn, J. Zimmerman, Acta Mater., 54 (2006) 643-653.
[18] W.G. Hoover, Phys. Rev. A, 31 (1985) 1695-1697.
[19] S. Nosé, J. Chem. Phys., 81 (1984) 511.
[20] Y. Mishin, M. Mehl, D. Papaconstantopoulos, A. Voter, J. Kress, Phys. Rev. B, 63 (2001) 224106.
[21] S. Plimpton, J. Comput. Phys., 117 (1995) 1-19.
[22] C. Kelchner, S. Plimpton, J. Hamilton, Phys. Rev. B, 58 (1998) 11085-11088.
[23] H.F. Zhan, Y.T. Gu, P.K.D.V. Yarlagadda, Adv. Sci. Lett., (2011 In press).
[24] W. Liang, M. Zhou, J. Eng. Mater. Technol., 127 (2005) 423-433.